Superconductivity and transport properties in ultrathin epitaxial single-crystal niobium films

1990 J. Phys.: Condens. Matter 2 3567

(http://iopscience.iop.org/0953-8984/2/15/013)

J. Phys.: Condens. Matter 2 (1990) 3567–3578. Printed in the UK

Superconductivity and transport properties in ultrathin epitaxial single-crystal niobium films*

Q D Jiang, Y L Xie, W B Zhang†, H Gu†, Z Y Ye, K Wu, J L Zhang, C Y Li and D L Yin‡

Department of Physics, Peking University, Beijing 100871, People's Republic of China

Received 20 March 1989, in final form 31 October 1989

Abstract. Pure and high-quality single-crystal Nb(001) thin films with thicknesses ranging from 40 Å to 1000 Å were grown epitaxially on NaCl(001) substrates by an UHV e-beam evaporation technique. TEM observations, resistivity and superconducting transition temperature measurements were carried out. A drastic fall-off in transition temperature and conductivity was observed in ultrathin single-crystal Nb films. The results are discussed within the framework of the existing theories and a strain-induced 'double-layer' model is proposed. Data for polycrystalline Nb thin films on glass substrates deposited under exactly the same evaporation conditions as the single-crystal films are also presented for comparison.

1. Introduction

Recently considerable interest has been generated in thin niobium films [1–12]. Because niobium has the highest T_c of the pure metals, several studies have been done on the mechanisms of T_c suppression with film thickness reduction [5–7], considering the competition between superconductivity and 2D Anderson weak localisation and enhanced Coulomb interaction effects [5–9].

Until the early 1980s, most experimental data of T_c suppression were interpreted in terms of the proximity effect due to the existence of a surface sheath of degraded superconductivity [10–11]. In the late 1970s and early 1980s it was also realised that weak localisation and interaction effects may play a prominent role in the properties of highly disordered thin superconducting films [13]. Experiments were carried out by Graybeal and Beasley [14] and Raffy *et al* [15] on amorphous Mo–Ge and W–Re superconducting thin films, respectively. Good agreements between their T_c suppression and the theory of Maekawa and Fukuyama [13] based on interaction effects in 2D disordered systems were found. The experimental data of Quateman [7] confirmed their results. However, Moehlecke and Ovadyahu [9] argued that the physical mechanisms responsible for the weakening of superconductivity remained rather obscure and there was no conclusive evidence that localisation effects played an important role in suppressing superconductivity in their Nb thin films. Recently, Park and Geballe [5] proposed that the T_c

* Work supported by the National Science Foundation of the People's Republic of China.

† Graduate Students.

‡ Special Member of CCAST (World Laboratory).

0953-8984/90/153567 + 12 $03.50

depression observed in their superconducting Nb thin films as the thicknesses were reduced could be attributed to the following effects: the proximity effect, the lifetime broadening effect and the weak localisation effect.

However, research so far has been done only on polycrystalline films, in which large variations can exist in their properties due possibly to their different grain sizes, impurities, substrate temperatures and types of substrates. Therefore, it is desirable to investigate their properties by using pure and high-quality single-crystal thin films.

In this paper, we report in detail on the epitaxial growth of high-quality single-crystal Nb films deposited in UHV electron beam evaporation systems with thicknesses ranging from 40 Å to 1000 Å, including transmission electron microscopy (TEM) observations, transport properties and transition temperature studies. In section 2, some useful theoretical considerations are briefly reviewed. Detailed sample preparation and measurements are described in section 3, with results in section 4. In section 5, the theories presented in section 2 and a model proposed in this paper are applied to explain the data. Finally, conclusions are summarised in section 6.

2. Theoretical considerations

2.1. Effect of weak localisation on resistivity

The scaling theory [16] predicts that in 2D disordered metallic systems all electrons in ground states will become localised, however weak the disorder. The precursor of this so-called weak localisation (WL) effect results in a logarithmic correction to the conductivity at finite temperature:

$$\Delta\sigma_{\square}^{L} = -(\Delta R_{\square})/(R_{\square}^{2}) = [\alpha' \log(T/T_0)]/R_{2D} \tag{1}$$

where $R_{2D} = \pi h/e^2$, $R_{\square}$ is the sheet resistance of the sample and α' is a constant.

2.2. Mechanisms of T_c suppression

2.2.1. The proximity effect. Cooper [17] proposed that due to the long superconducting coherent length, there is a finite probability for Cooper pairs extending into the normal metal (N) from the superconducting metal (S) when S is brought in intimate contact with N. This will result in a reduction in the effective interaction $(N(0)V)$ of the NS system. The above idea was extended by DeGennes [18] who obtained the following formula for the effective value of $N(0)V$ in the Cooper limit $\xi_S \gg d_S$ and $\xi_N \gg d_N$:

$$(N(0)V)_{\text{eff}} = [(N(0)^2V)_N d_N + (N(0)^2V)_S d_S]/[N(0)_N d_N + N(0)_S d_S] \tag{2}$$

where the subscripts denote the relevant quantity in S (or N), ξ and d are coherence length and thickness, respectively. From equation (2) and the BCS T_c formula

$$T_c = (\theta_D/1.45)\exp[-1/(N(0)V)_{\text{eff}}] \tag{3}$$

it is clear that the value of T_c for the NS system will fall off almost exponentially with decreasing d_S. (In equation (3) θ_D is the Debye temperature.)

2.2.2. The Maekawa–Fukuyama theory. Maekawa and Fukuyama [13] studied the effects of localisation on 2D superconductivity theoretically. The theory predicted that

an enhanced Coulomb interaction between electrons produced by localisation effects resulted in a depression of T_c as is expressed in equation (4),

$$\log(T_c/T_{c0}) = -\gamma(\tfrac{1}{2}\beta^2 + \tfrac{1}{3}\beta^3) \tag{4a}$$

where

$$\gamma = (g_1 N(0) e^2 R_\square)/\pi h \qquad \beta = \log[(5.5 T_{c0}\,\xi_0)/T_c L]. \tag{4b}$$

Here T_c and T_{c0} are the transition temperatures of films with and without impurity scattering, ξ_0 is the zero-temperature coherence length corresponding to T_{c0} and L is the mean-free path associated with elastic scattering. The factor g_1 is a positive coupling constant related to the Coulomb interaction. In equation (4*a*) the first term is due to reduction of the density of states and the second term is due to a correction to the electron–electron interaction.

2.2.3. The density of states broadening effect. Many authors have studied the universal correlation between resistivity and T_c in A15 compounds and in transition metals [19, 20]. In the following we describe briefly the model introduced by Testardi and Mattheiss [20]; increasing resistivity causes a progressive smearing of the peak in the single-particle electron density of states at the Fermi level, which in turn results in a reduction in the effective density of states:

$$\langle N(E)\rangle = \int N(E) S(E_b)\,\mathrm{d}E \tag{5a}$$

where

$$E_b = h/(2\pi\bar{\tau}) \qquad \text{and} \qquad \rho \propto \bar{\tau}^{-1}. \tag{5b}$$

$S(E_b)$ is a broadening function and ρ is the resistivity corresponding to an averaged lifetime $\bar{\tau}$. Combining equation (5) and the McMillan expression for T_c [21],

$$T_c = \frac{\theta_D}{1.45}\exp\left(-\frac{1.04(1+\lambda)}{\lambda - \mu^*(1+0.62\lambda)}\right) \tag{6}$$

it is obvious that increasing resistivity will suppress T_c providing that λ is proportional to $\langle N(E)\rangle$. In expression (6) λ and μ^* are the electron–electron coupling constant and the screened Coulomb potential, respectively.

3. Sample preparation and measurement

The substrates used in this study were fresh air-cleaved single-crystal NaCl(001) and glass for comparison. In order to reduce the internal strain, prior to cleavage the NaCl was annealed at 400 °C in a vacuum of 10^{-3} Torr for five to eight hours and furnace-cooled down to room temperature. All the glass substrates underwent a rigorous ultrasonic cleaning. The deposition took place in a Balzers UMS 500P double-gun electron beam evaporation system equipped with a microprocessor. Before deposition, the chamber and substrates were baked for several hours. The sources were then outgassed by evaporating for a few minutes thereby also forming a gettering layer inside the chamber. Then Nb films with thicknesses ranging from 40 Å to 1000 Å were deposited simultaneously onto NaCl and glass substrates. To prevent Nb from oxidising upon completion

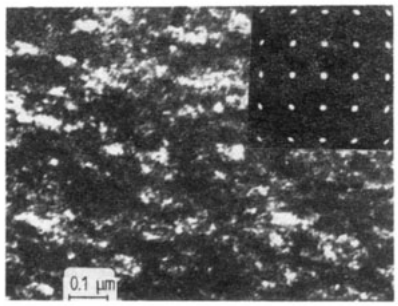

Figure 1. Typical dark-field (110 beam) electron microscopy of Nb thin film with $d = 500$ Å on NaCl(001) substrate; the inset is the electron diffraction pattern.

of the Nb deposition, each sample was covered with a 30 Å layer of silicon. Such a deposition procedure was similar to that described by Park and Geballe in [5]. Using the mask technique, a well-defined geometry (2×8 mm^2) was produced and subsequently four copper strips (with widths of less than 0.2 mm) were deposited to form electrical contacts for four-terminal measurements.

All the films were prepared under the same condition of substrate temperature 150 °C, deposition rate 2 Å s^{-1} and vacuum $(2.3–3.8) \times 10^{-8}$ Torr during deposition. Both rates and film thicknesses were determined by a calibrated quartz crystal monitor.

Samples were examined by TEM and electron diffraction, which determined the microstructure, lattice constant and epitaxial relationship with the substrate.

The values of the resistance and T_c were measured by a four-terminal DC resistance technique. Samples were clamped to a copper block, in which were imbedded a calibrated Lake Shore Cryotronics germanium thermometer and a Lake Shore Cryotronics silicon diode thermometer. The block itself was also a small ^{4}He pot that could be pumped to 1.9 K. Four leads were indium soldered to the copper contacts. The measuring current was 2.5 μA or 10 μA for samples with thicknesses below or above 80 Å, respectively.

4. Experimental results

4.1. Structure

Figures 1 and 2(*a*) show the typical dark-field TEM of Nb films with $d = 500$ Å and 40 Å on the NaCl(001) substrates. The insets show the corresponding electron diffraction patterns. It is obvious from figures 1 and 2(*a*) that high-quality single-crystal BCC Nb thin films can be grown epitaxially on single-crystal NaCl(001) substrates at a relatively low temperature (150 °C), even at a thickness of 40 Å. The TEM bright-field image of the sample with $d = 40$ Å showed quite a uniform contrast without islands or clusters (figure 2(*b*)). We therefore believe the films are uniform so that the measurements reflect an intrinsic dependence on thickness rather than indicating inhomogeneities or breaks in the thin films. The epitaxial relationship with NaCl is found from high-resolution electron diffraction (HRED) observations to be:

$$\text{Nb}(001) \parallel \text{NaCl}(001) \qquad \text{and} \qquad \text{Nb}[110] \parallel \text{NaCl}[100]. \tag{7}$$

Measurements show that for Nb films with $d = 40$ Å the lattice constant is 3.39 ± 0.02 Å, 2.7% larger than that of thick films with d above 120 Å and that of bulk samples, which

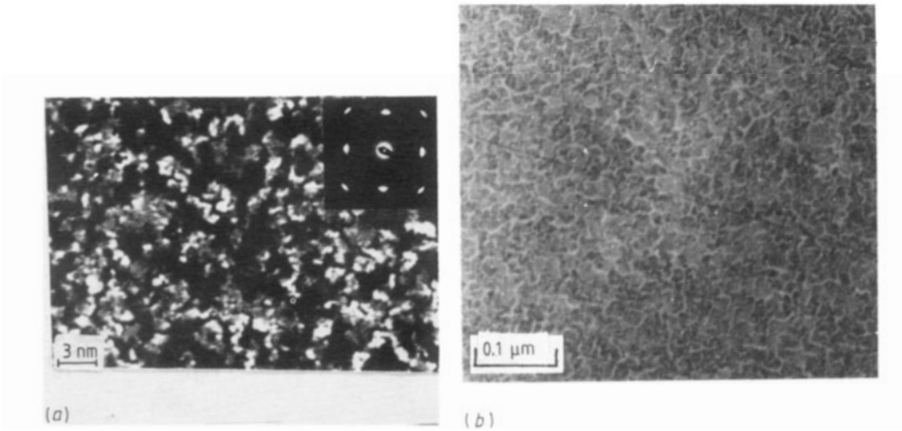

Figure 2. (*a*) Typical dark-field (110 beam) electron microscopy of Nb thin film with d = 40 Å on a NaCl(001) substrate; the inset is the electron diffraction pattern. (*b*) The TEM bright-field image for a single-crystal Nb thin film with d = 40 Å on a NaCl(001) substrate.

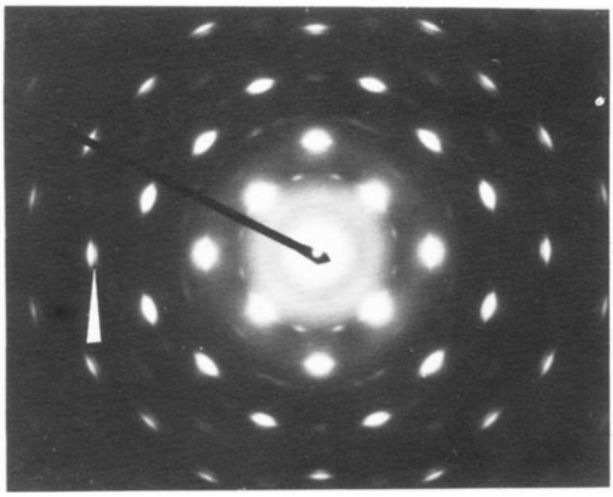

Figure 3. Electron diffraction pattern for a Nb film with d = 80 Å on a NaCl(001) substrate. Note the two sets of spots which correspond to a_0 = 3.39 Å and a_0 = 3.30 Å BCC Nb.

is 3.30 ± 0.02 Å. It is interesting to note that two sets of spots, which correspond to BCC Nb with different lattice constants of 3.39 Å and 3.30 Å, were observed in the same electron diffraction pattern for films with d = 80 Å (figure 3). To our knowledge this is the first observation of different lattice constants coexisting in the same epitaxial single-crystal Nb films. Moreover, the Nb lattice expansion in ultrathin films on NaCl(001) is surprisingly large. A similar lattice constant expansion to 3.350 Å was observed by Claassen *et al* [1] in a thin (50 Å) Nb(100) film epitaxially grown on ($1\bar{1}02$) sapphire substrates. As will be discussed below, the large strain in the epitaxial Nb films results in anomalous transport and superconducting properties.

4.2. Resistivity

The thickness dependence of the resistivity in epitaxial single-crystal Nb films is very different from that in polycrystalline films deposited on glass substrates under exactly

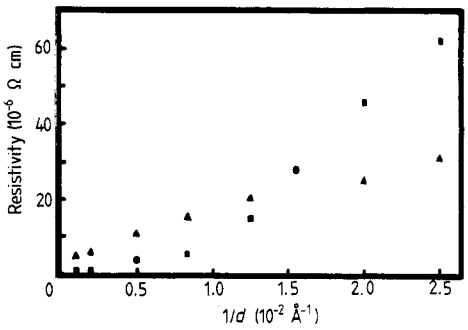

Figure 4. Residual resistivity ρ_{10K} as a function of $1/d$ for Nb films on NaCl (■) and on glass (▲) substrates.

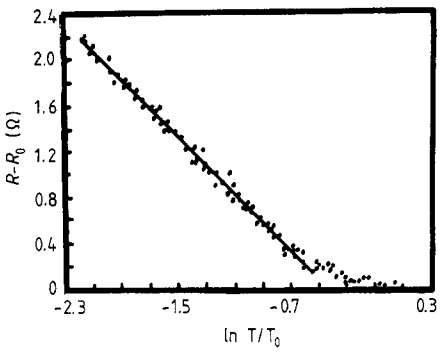

Figure 5. Ln T dependence of resistance in epitaxial Nb film with $d = 40$ Å.

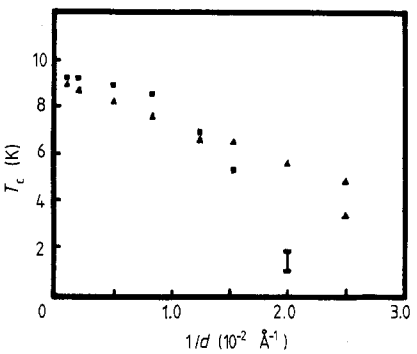

Figure 6. T_c as a function of $1/d$ for single crystal (■) and polycrystalline (▲) Nb thin films.

the same evaporation conditions. Results shown in figure 4 indicate that for a thickness greater than 80 Å, that the resistivity of the epitaxial films is lower than that of the corresponding polycrystalline ones. In the latter case, the resistivity varies linearly with $1/d$ (d is film thickness). Below 80 Å, the resistivities of the epitaxial films tend to increase in a much quicker way with decreasing d. For a single-crystal Nb film with $d =$ 1000 Å, the residual resistance ratio (RRR) is 30 (corresponding to a mean-free path of 830 Å at low temperatures) which is ten times the RRR in a polycrystalline film with the same thickness. Such a high value of the RRR is further evidence that the samples in this study are high-quality single-crystal epitaxial films.

The temperature dependence of the resistivity in epitaxial ultrathin films is also different from that in non-epitaxial polycrytalline films. All non-epitaxial films are metallic and superconducting even for the films with $d = 40$ Å ($T_c = 3.4$ K). However, in the case of epitaxial films with $d = 50$ Å, a negative temperature coefficient of resistivity below 10 K and a sudden superconducting transition near 2 K are observed. The transition is not complete at the lowest achievable temperature of 1.9 K in our experimental set-up. For ultrathin epitaxial films with $d = 40$ Å, the superconducting transition disappears completely down to 1.9 K and a ln T increase in resistivity with decreasing temperature occurs as shown in figure 5.

4.3. Transition temperature T_c

T_c for an epitaxial film with $d = 1000$ Å was measured to be 9.3 K, the same value as that of the bulk sample. T_c as a function of $1/d$ is shown in figure 6. Results for Nb films on glass substrates are also given for comparison. It is obvious that the value of T_c for epitaxial films deviates from the linear dependence on $1/d$ which was observed for non-epitaxial polycrystalline films in this study and other works [6, 7]. Above 80 Å, the value of T_c for films on NaCl increases slightly with d, however, it falls off drastically with d near and below 80 Å. Similar behaviour has been observed in Nb films deposited on single-crystal Si substrates in [10]. The error bar in figure 6 is an estimated value of T_c due to the incomplete transition for a film with $d = 50$ Å. Comparison of figure 4 with figure 6 shows that the drastic decrease in T_c corresponds to a similar change in the resistivity for single-crystal Nb films. As shown above, below 80 Å there is a large strain in the epitaxial films. So the differences of the resistivity and value of T_c from non-epitaxial polycrystalline films may result from the strain in epitaxial films. The mechanisms governing the suppression of T_c both in single crystalline and polycrystalline Nb films will be discussed further below.

5. Discussion

5.1. Epitaxial growth

The striking feature of the results in this work is the co-existence of different lattice constants in one epitaxial Nb thin film. The calculated mismatch between the NaCl lattice ($a_s = 5.63$ Å) and the Nb lattice ($a_0 = 3.30$ Å) is about 0.2. Moreover, epitaxial growth can occur even with such a large misfit between the substrate and the overlayer. This phenomena can be understood within the framework of the coincidence boundary model in epitaxial growth theory [22].

According to this model, if the lattice misfit is very large and the parameters satisfy the following conditions:

$$a_0/a_s = m/n \qquad \text{and} \qquad n = m \pm 1 \tag{8}$$

where n and m are integers, then the interface can be divided into units of length ma_s (or na_0). In some of the units overgrowth atoms strain to lie at atomic sites in the substrate and in the other units interfacial dislocations with Burgers vector of $\pm a_0/m$ (or $\pm a_s/n$) are generated. That is, the lattice mismatch between overlayer and substrate is accommodated by elastic strain and misfit dislocations. As is predicted by the theory, there exists a critical thickness h_c:

$$h_c = \frac{G_s(1-\nu)}{2(G_0+G_s)(1+\nu)}\frac{a_0}{mF} \tag{9}$$

with

$$F = (ma_s - na_0)/na_0 \tag{10}$$

where G_s is the shear modulus and ν is the Poisson ratio. When the thickness of the overlayer is below h_c, then most of the mismatch is accommodated by elastic strain and a coherent coincidence boundary is expected. When the thickness of the overlayer is above h_c, the mismatch is then shared by elastic strains and misfit dislocations. Based on

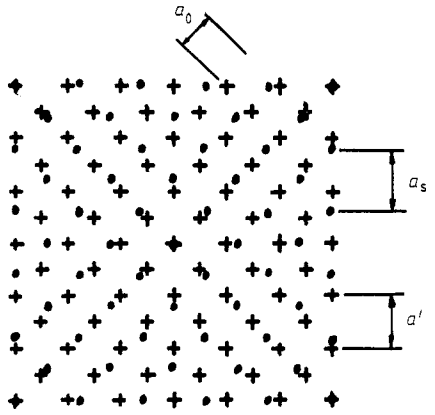

Figure 7. Overlays of Nb atoms on NaCl lattice sites according to the epitaxial relationships (see text): ●, NaCl lattices; +, Nb lattices.

our observed epitaxial relationship (7) and the model described above, the lattice overlayers of Nb on NaCl are shown in figure 7. Note that a value of $\sqrt{2}a_0$ (a') instead of a_0 itself should be used in equations (9) and (10). Since $a_s/a' = 1.206 \approx \frac{6}{5}$, it is easy to calculate the effective misfit to be 0.5%, which is very small. Moreover, it is interesting to notice that the strained-lattice constant ($a_0' = 3.39$ Å) of the film with $d = 40$ Å still satisfies the condition of equation (10), with $a_s/(\sqrt{2}a_0') = 1.167 \approx \frac{7}{6}$. This may explain the fact that the strained-lattice constant is 3.39 Å instead of any other value. We suppose that the lattice constant of 3.39 Å may be found for films with thickness below h_c.

For a rough estimate of h_c, assuming $G_0 = G_s$ and $\nu = \frac{1}{3}$ in equation (9), we obtain the lower limit of h_c to be 23 Å (generally $G_0 > G_s$). Since the lattice constant of NaCl, a_s, is much larger than a' (see figure 7), the above estimate indicates that Nb films with d below h_c tend to strain elastically to produce a coherent interface on the NaCl(001) face, therefore the Nb lattice tends to expand. For films with d above h_c, the generation of misfit dislocations is energetically favourable and the normal lattice constant (or one slightly expanded) will be expected. The picture described above agrees qualitatively with our TEM findings. However, the value of h_c estimated above is somewhat smaller than the observed value, which is around 40 Å. The discrepancy may originate from the oversimplification of this model where the orthogonal 2D sets of interfacial dislocations were assumed in reference [22] to calculate the dislocation energy.

5.2. Size effect on resistivity and weak localisation

Resistivity as a function of films thickness is expected to vary linearly with $1/d$ by both the usual size effect theory [23] and the grain boundary scattering theory [24]. This is the case for our data of polycrystalline films (figure 4). However, this is not the case for our epitaxial single-crystal Nb films. Large deviations from a linear dependence of $1/d$ are evident from figure 4, especially in the thickness range below approximately 80 Å. As was shown in section 5.1, there exist large strains in epitaxial films with thicknesses below 80 Å. This may suggest that the 'anomalous' thickness dependence of resistivity for epitaxial single-crystal Nb films possibly results from the lattice strain in the films.

The observed logarithmic temperature dependence in resistivity for ultrathin single-crystal Nb films with $d = 40$ Å is fitted to the weak localisation correction expressed in equation (1), with α' in equation (1) being found to be 1.08, which is in close agreement

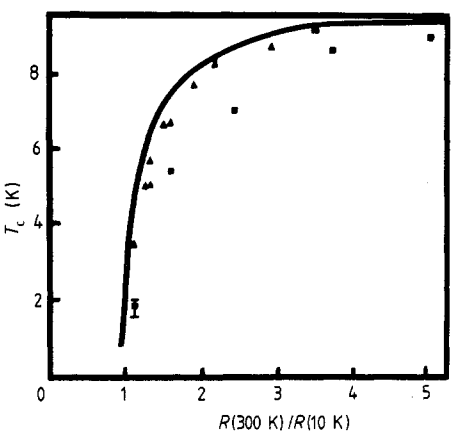

Figure 8. T_c as a function of residual resistivity ratio for single-crystal (■) and for polycrystalline (▲) Nb films. The full curve shows the results for N^+-implanted Nb films [26].

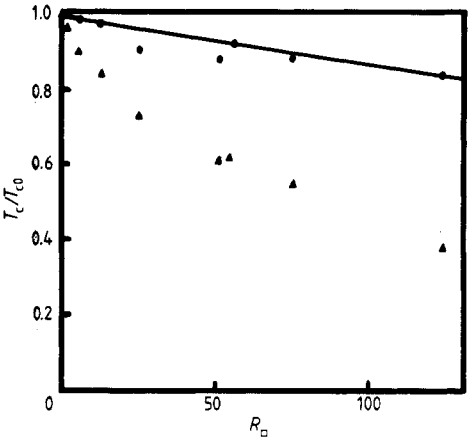

Figure 9. T_c/T_{c0} as a function of sheet resistance for polycrystalline Nb films without (▲) and with (●) BRE correction (see text).

with both the theoretical value of $\alpha' = 1$ for non-interacting spin systems and the experimental value of $\alpha' = 1.1 \pm 0.1$, reported by Moehlecke and Ovadyahu [9]. It is worth noticing that although the sheet resistance of our sample (154 Ω), is much smaller than that of Moehlecke's experiment (4.56 kΩ), both experiments give the same value of α'. These results indicate that the value of α' obtained is independent of the sheet resistance as is predicted by the weak localisation theory.

5.3. T_c suppression

Since our Nb films were deposited at a substrate temperature of 150 °C and a 30 Å Si layer was coated on the surface to prevent Nb from oxidation, following Park and Geballe [5], we believe that proximity effects due to an oxidised layer are reduced so that they are the smallest contribution to the T_c fall-off in both polycrystalline and single-crystal films. However, it will be seen below that a proximity effect due to the strained layer can make a dominant contribution to T_c suppression in epitaxial films. Reasonably, we shall eliminate the former contribution in the following analysis.

We estimate first the contribution from the lifetime broadening effect [20] (we hereafter refer to this as a bulk resistivity effect or BRE). It is interesting to compare our T_c data with those of N^+-implanted thick Nb films with $d = 2000$ Å, in which Camerlingo *et al* [25] have shown that the fall-off in T_c with increasing residual resistivity ρ_0 results mainly from the BRE. Figure 8 shows T_c plotted against the residual resistivity ratio (RRR) for our polycrystalline (▲) and single crystalline (■) Nb films. The full curve shown is the data from Camerlingo *et al*. Our data points for polycrystalline samples almost fall on the same curve of implanted films indicating that the same mechanism of BRE governs the T_c suppression in evaporated polycrystalline and N^+-implanted Nb thin films. Note that our data points are slightly off the curve. This implies that there exists a small contribution from other effects to be discussed below.

In the limit of $R_\square \ll R_{2D}$ the Maekawa and Fukuyama [13] theory leads to a proportional decrease of T_c/T_{c0} as a function of sheet resistance $R_\square$. Conveniently we plot

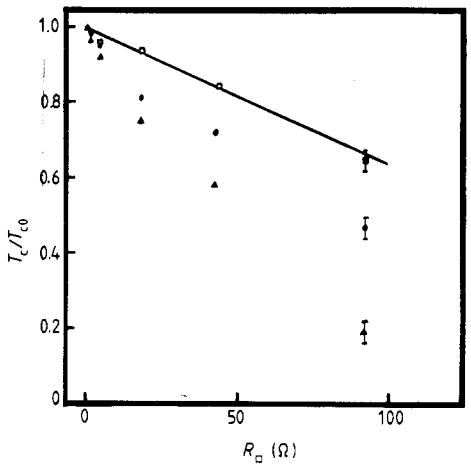

Figure 10. T_c/T_{c0} as a function of the sheet resistance for single-crystal Nb films without (▲) and with (●) BRE correction, and after BRE and proximity effect corrections (□) (see text).

T_c/T_{c0} against $R_\square$ in figure 9. Care should be taken in choosing T_{c0} for comparing experimental and theoretical results. Since thickness reduction, as well as resistivity increase, result in an enhancement in $R_\square$, and T_{c0} in equation (4*a*) is itself a function of the residual resistivity, $T_{c0}(\rho_0)$, therefore, the BRE correction should be made before making an estimate of the contribution from the WL effect. In figure 9, such a correction is made by choosing $T_{c0}(\rho_0)$ in equation (4*a*) and in figure 9 from the value of T_c at ρ_0 in N^+-implanted Nb films (full curve in figure 8). This is reasonable because single BRE theory explained the experimental data of Camerlingo *et al* [26] fairly well. It is obvious from figure 9 that after the BRE correction the points of T_c/T_{c0} against $R_\square$ fall closely on the straight line that MF theory predicted.

Now we turn to analyse the epitaxial single-crystal films. In a similar manner to the polycrystalline samples, the BRE and WL effect corrections for epitaxial single-crystal samples are performed in exactly the same way. The results are shown in figure 10. It is apparent that data points deviate badly from the T_c–ρ_0 curves (figure 8) for polycrystalline and N^+-implanted Nb thin films and the straight line in figure 10. The important fact is that they all lie much below the curves. These suggest that apart from the BRE and WL effects other important mechanisms govern the further depression of T_c in the epitaxial single-crystal Nb films.

Recalling our discussions made above (section 5.1) on the striking structural features in the epitaxial Nb thin films, we suppose that epitaxial Nb films with d below 80 Å actually consist of two layers, namely, a superconducting layer S_1 (in S_1, $a_0 = 3.30$ Å), and a strained or low-T_c layer S_2 (in S_2, $a_0' = 3.39$ Å) with thickness d_2 ($d = d_1 + d_2$). As was pointed out in section 2, the existence of a low-T_c layer (S_2) will reduce the effective interaction $(N(0)V)_{\text{eff}}$ by virtue of the proximity effect, which in turn, will suppress the transition temperature. In the following analysis the bulk resistivity effect is formally attributed to the change in effective interaction $(N(0)V)_{S_1}$ of the S_1 layer. The following parameters are used in equation (2) to calculate $(N(0)V)_{\text{eff}}^{\text{theor}}$: $\theta_D = 279$ K, $(N(0)V)_{S_2} = 0.250$ and $N(0)_{S_2}/N(0)_{S_1} = 0.7$. Fitting the experimental data to equations (2) and (3) the value of d_2 is found to be 20 Å, which is surprisingly consistent with the calculated value of h_c of 23 Å inferred from the structural analysis in section 5. After taking account of the contributions from proximity and bulk resistivity effects, the

data for T_c/T_{c0} against $R_\square$ are shown again in figure 10 (□), which agree reasonably with the dependence on $R_\square$ that weak localisation theory predicted. Therefore, the further depression of T_c in epitaxial Nb films results from the proximity effect due to a strained low-T_c layer.

Alternatively, the experimental results may possibly be explained by breaks of continuity in our very thin epitaxial films [26, 27]. On the evidence of our microscopy, we believe the films to be homogeneous so that the measurements presented reflect an intrinsic thickness dependence.

6. Conclusions

The following conclusions can be drawn from the present study:

(*a*) Pure and high-quality single-crystal Nb(001) thin films down to $d = 40$ Å can be grown epitaxially on single-crystal NaCl(001) substrates at relatively low substrate temperatures.

(*b*) Large strains due to large lattice mismatch between Nb and NaCl play a dominant role in the drastic increase of resistivity of epitaxial single-crystal Nb films with thickness below about 80 Å.

(*c*) The lifetime broadening effect and Anderson weak localisation effect are responsible for the depression of T_c observed in non-epitaxial polycrystalline Nb films as the film thicknesses are reduced.

(*d*) In addition to the above two effects (*c*), the proximity effect due to the existence of the strained layer is another important factor that results in the further suppression of T_c in epitaxial Nb thin films.

Acknowledgments

The authors thank Professor Y D Dai for helpful discussions and Dr Q Li for her kind assistance in measurements.

References

[1] Claassen J H, Wolf S A, Qadri S B and Jones L D 1987 *J. Cryst. Growth* **81** 557
[2] Oya G I, Koishi M and Sawada Y 1986 *J. Appl. Phys.* **60** 1440
[3] Gavaler J R, Braginski A I, Janocko M A and Talvacchio J 1985 *Physica* **135B** 148
[4] Alessandrini E I, Laibowitz R B and Viggiano J M 1981 *J. Vac. Sci. Technol.* **18** 318
[5] Park S I and Geballe T H 1985 *Physica* **135B + C** 108
[6] Park S I and Geballe T H 1986 *Phys. Rev. Lett.* **57** 901
[7] Quateman J H 1986 *Phys. Rev.* B **34** 1948
[8] Dalrymple B J, Wolf S A, Ehrlich A C and Gillespie D J 1986 *Phys. Rev.* B **33** 7514
[9] Moehlecke S and Ovadyahu Z 1984 *Phys. Rev.* B **29** 6203
[10] Kodama J I, Itoh M and Hirai H 1983 *J. Appl. Phys.* **54** 4050
[11] Wolf S A, Kennedy J J and Nisenoff M 1976 *J. Vac. Sci. Technol.* **13** 145
[12] Mayadas A F, Laibowitz R B and Cuomo J J 1972 *J. Appl. Phys.* **43** 1287
[13] Maekawa S and Fukuyama H 1981 *J. Phys. Soc. Japan* **51** 1380
[14] Graybeal J M and Beasley M R 1984 *Phys. Rev.* B **29** 4167
[15] Raffy H, Laibowitz R B, Chaudhari P and Maekawa S 1983 *Phys. Rev.* B **28** 6607
[16] Anderson P W, Abrahams E and Ramakrishan T V 1979 *Phys. Rev. Lett.* **43** 718

[17] Cooper L N 1961 *Phys. Rev. Lett.* **6** 689
[18] DeGennes P G 1964 *Rev. Mod. Phys.* **36** 225
[19] Gurvitch M 1983 *Phys. Rev.* B **28** 544
[20] Testardi L R and Mattheiss L F 1978 *Phys. Rev. Lett.* **41** 1612
[21] McMillan W L 1968 *Phys. Rev.* **167** 331
[22] Matthews J W 1979 *Dislocations in Solids—Dislocation in Crystals* vol 2, ed F R N Nabarro (Amsterdam: North-Holland) p 466
[23] Fuchs K 1938 *Proc. Camb. Phil. Soc.* **34** 100
[24] Mayadas A F and Shatzkes M 1970 *Phys. Rev.* B **1** 1382
[25] Camerlingo C, Scardi P, Tosello C and Vaglio R 1985 *Phys. Rev.* B **31** 3121
[26] Deutscher G 1984 *Percolization, Localization, and Superconductivity* ed A M Goldman and S A Wolf (New York: Plenum) p 95, and references therein
[27] Palevski A, Rappaport A M, Kapitulnik A, Fried A and Deutscher G 1984 *J. Phys. Lett.* **45** L367